Available online at www.sciencedirect.com
ScienceDirect
International Journal of Heat and Mass Transfer 51 (2008) 4121–4131
International Journal of HEAT and MASS TRANSFER
www.elsevier.com/locate/ijhmt

Numerical modelling of metal droplet cooling and solidification

N. Zeoli, S. Gu *, S. Kamnis

School of Engineering and Applied Science, Aston University, Aston Triangle, Birmingham B4 7ET, United Kingdom

Received 8 November 2006
Available online 21 February 2008

Abstract

In an atomisation process for power production, metal droplets go through undercooling, recalescence, peritectic and segregated solidification before fully solidified. The cooling process is further complicated by droplet break-up during the atomisation. This paper describes a numerical model which combines both cooling and break-up in a single computation. The dynamic history of droplets is solved as discrete phase in an Eulerian gas flow. The coupling between droplet and gas flows are two-way, in which the heat and momentum exchanges affecting the gas flow are treated as source/sink terms in the fluid equations. The droplet model is employed to a gas atomisation process for metal powder production and good agreement is achieved with the results in open literature. The model results further confirm that thermal history of particles is strongly dependent on initial droplet size. Large droplets will not go through undercooling while small droplets have identifiable stages of undercooling, unclearation and recalescence. The predictions demonstrate that droplets have very similar profiles during gas atomization and the major factor influencing the atomization and solidification process of droplets are in-flight distance.

Keywords: Gas atomisation; Cooling; Solidification; Heat transfer; Metal powder; Break-up

1. Introduction

Gas atomisation technology has been widely employed to produce fine spherical metal powders commercially. In a typical powder production process such as close coupled gas atomization, hot liquid metal stream has extensive heat and momentum exchange with high pressure cold gas jets, which give rise to high cooling rate (10^2–10^4 °C/s) [1] and deep under-cooling to the atomised metal droplets. The produced powder particles have reduced segregation and very fine microstructure which improves material properties such as strength, toughness, hardness and corrosion resistance. The two key mechanisms associated with gas atomisation process are break-up (where the melt is atomised into droplets) and cooling (where droplets are solidified to powder particles). The production of metal powder is interplay of these two mechanisms, i.e., heat is transferred from melts to atomising gases as droplets form and solidify. It is important to have good understanding of both mechanisms of gas and melt interaction in order to improve the product yield and control the production process. The complex nature of gas atomisation process has imposed some great challenges to research community. A survey of the relevant literature shows that no detailed experimental data are currently available to demonstrate the atomisation and thermal history of droplets during the process. Numerical modelling is believed to be an effective approach to examine the underlying thermal-physics of powder atomisation and numerous mathematical models have been developed for powder atomisation over last decade. However, most numerical models only simulate the gas flow which cannot provide insight information of metal droplet evolution and thermal history. Therefore, it is important to examine the thermal history of individual powder droplets. Among the limited work of modelling metal droplet behaviour [1–5], the coupling of gas and droplets is normally treated as one-way, i.e., the presence of droplets has no effect on the gas flow field in terms of

* Corresponding author. Tel.: +44 (0) 1212043582; fax: +44 (0) 1212043683.
E-mail addresses: zeolin@aston.ac.uk (N. Zeoli), s.gu@aston.ac.uk (S. Gu).

0017-9310/$ - see front matter © 2008 Elsevier Ltd. All rights reserved.
doi:10.1016/j.ijheatmasstransfer.2007.11.044

Nomenclature

A	oscillation amplitude
B_0, B_1	constants for KH model
C_b, C_F, C_k, C_d	constants for TAB model
c_g	specific heat of gas
c_{pl}	specific heat of the material in the liquid state
c_{ps}	specific heat of the material in the solid state
c_0	composition
d_p	droplet radius
f	solid fraction inside droplet
h	convective heat transfer coefficient
h_f	melt latent heat of fusion
k	Boltzmann's constant
k_g	gas thermal conductivity
Pr	Prandtl number
R	solid–liquid interface mobility
r	diameter of child droplet
r_p	diameter of parent droplet
Re	Reynolds number
$\dot{T}$	cooling rate
T_g	gas temperature
T_L	liquidus temperature
T_M	reference temperature
T_N	nucleation temperature
T_p	droplet temperature
T_{per}	peritectic temperature
T_w	wall temperature
ΔT_{het}	heterogeneous undercooling
ΔT_{hom}	homogeneous undercooling
t	time
t_b	break-up time
t^n	time step n
u_{rel}	relative velocity between gas and droplet
V	particle volume
Z	Ohnesorge number ($=v(\rho/\sigma\, dp)$)
x	displacement of the droplet equator
y	non-dimensional value for the displacement of the droplet equator
y^n	y value at t_n
We	Weber number
Γ	Taylor number ($=Z(We\,0.5)$)
ε	emissivity
Λ	wavelength of disturbance
μ_g	molecular viscosity of the gas
μ_l	liquid viscosity
ρ_p	droplet density
ρ_g	gas flow density
ρ_l	melt flow density
Σ	surface tension of the fluid droplet
σ_m	solid liquid interface energy
σ_{SB}	Stefan–Boltzmann constant
ϕ	intermediate parameter used for break-up time model
Ψ	oscillation amplitude
Ω	growth rate of the wavelength
Ω_V	atomic volume of the material
ω	oscillation frequency

heat and momentum sources. This is because the gas flow is not solved but is assumed as an exponential correlation for the gas velocity distribution. More realistic models with two-way coupling between gas and powder flows have been used in [6,7], but their prediction is limited by the assumption of constant droplet size throughout the computation without droplet break-up.

The formation of individual powder particle is a result of heat transfer process in microscale. The study of metal droplet cooling [6] reveals that metal droplets endure undercooling, recalescence, peritectic and segregated solidification. Existing droplet models have not yet incorporated the complete thermal behaviour of droplet cooling in such details. For example, the droplet models in [1,2] assume that solidification ends after peritectic transformation while study has shown the evidence of further segregated solidification after peritectic transformation [6]. Another important factor has been largely ignored for droplet modelling is the droplet break-up while nearly all the existing droplet models have used uniform droplet size throughout the computation. Most recently, progress has been made to develop atomisation model for metal droplets [8] by incorporating break-up mechanism such as Taylor analogy break-up (TAB) and Kelvin–Helmotz (KH) instability theories. That droplet model is able to depict the evolution of droplet geometry and thermal profile during the atomisation. This pioneering modelling work provides a step-forward solution to quantitatively describe the droplet history during atomisation. The limitation with that droplet model lies in the internal heat transfer model which cannot accurately present the complicated cooling behaviour of alloys.

This paper describes a heat transfer model which incorporates the complete thermal behaviour of metal droplet cooling including undercooling, recalescence, peritectic and segregated solidification. Segregated solidification is solved with Scheil's equation [9] in this paper. Although more sophisticated models, such as the Brody–Flemings theory, the Bower–Bordy–Flemings theory and the Clyne–Kurz Theory are currently available, Scheil's solutions have been found to give similar predictions despite its simplicity [1]. The heat transfer model is fully integrated with the droplet break-up model described in [8], in this way, both the break-up and thermal behaviour within droplets are calculated simultaneously. The combination of break-up and heat transfer models is important to understand the powder atomisation process, i.e., the thermal behaviour of droplets and the powder size distribution are strongly correlated as a result of break-up and cooling. The coupling between the

metal droplets (Lagrangian tracking) and the atomising gas flows is two-way, i.e., the heat and momentum exchanges affecting the fluid flow are treated as source/sink terms in the fluid equations, therefore the gas flow pattern includes any possible effect from droplet phase. The gas flow is computed using the commercial finite element software Fluent [10]. The droplet cooling and break-up models have been implemented as user defined functions (UDF) in the discrete phase model (DPM) available in Fluent. In order to achieve a good accuracy of the solution, the time scale adopted is 10^{-6} s (which gives the possibility to reproduce recalescence) and the grid size is adapted until no significant changes are detected in the transport phenomena. This paper is focused on the droplet modelling and the details of gas flow simulation can be found in [8].

2. Mathematical models

The combination of droplet cooling and break-up is achieved through a UDF as shown schematically in Fig. 1. The models are described as follows.

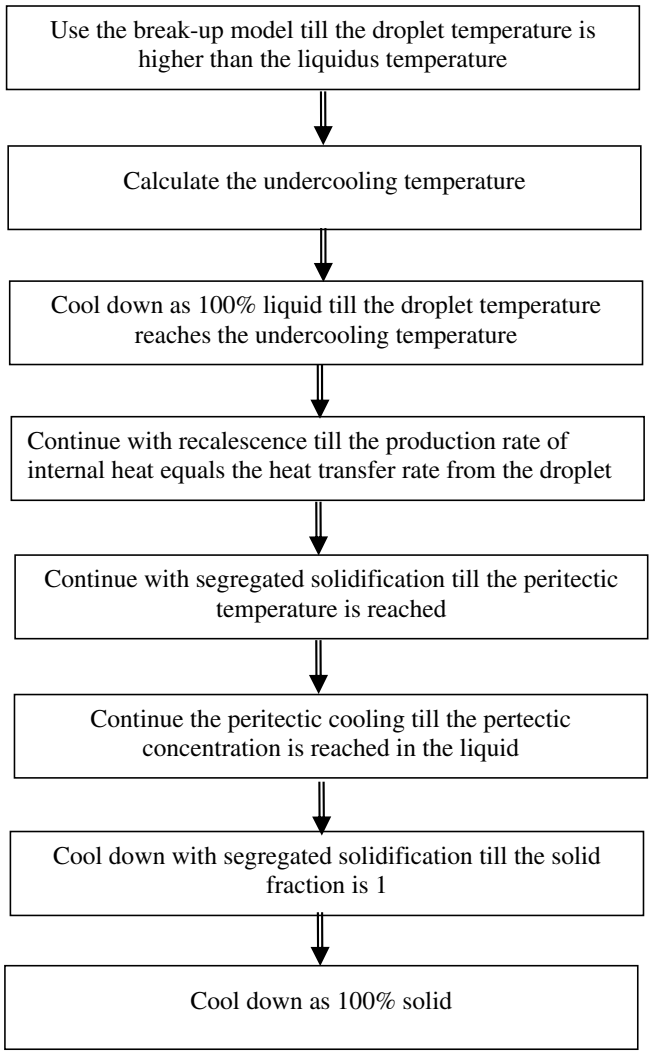

Fig. 1. Flow chart of model coupling in UDF.

2.1. Droplet cooling model

Most metal powders produced by gas atomisation are alloy rather than pure metal. In the current analysis, the modelling is based on a particular alloy γ-TiAl [11] and its phase diagram is shown in Fig. 2, however, the cooling model can be applied to other material composition given the correct thermal parameters. The cooling process for a metal droplet in an environment similar to gas atomisation has been best described in [6]. A complete transformation from liquid droplet to solid particle includes: cooling in liquid state, undercooling, recalescene, initial segregated solidification, peritectic transformation, further segregated solidification and cooling in solid state. An accurate representation of the cooling process needs to include all the sub-process which is described, respectively, as follows.

2.1.1. Cooling in liquid state

When droplets are just formed after they break away from the melt stream, the droplets are superheated with temperature above the liquidus temperature T_L. As the liquid droplets are cooled down by the surrounding gas, the heat exchange as a result of convection and radiation can be described as

$$c_{pl}\frac{dT_p}{dt} = \frac{6h}{\rho_p d_p}(T_p - T_g) - \frac{6\varepsilon\sigma}{\rho_p d_p}(T_p^4 - T_w^4). \quad (1)$$

2.1.2. Undercooling

Eq. (1) is valid for droplets in liquid state (liquid cooling and undercooling) when droplet temperature declines from superheated to liquidus temperature and further decreases to nucleation temperature. The period from liquidus to nucleation temperature is undercooling. In the context of high pressure gas atomisation, droplets are surrounded by large volume of cold gas. The extensive heat exchange between hot droplets and cold surrounding gas may give rise to undercooling of droplets. It is known that undercooling is a function of the cooling rate and droplet diameter.

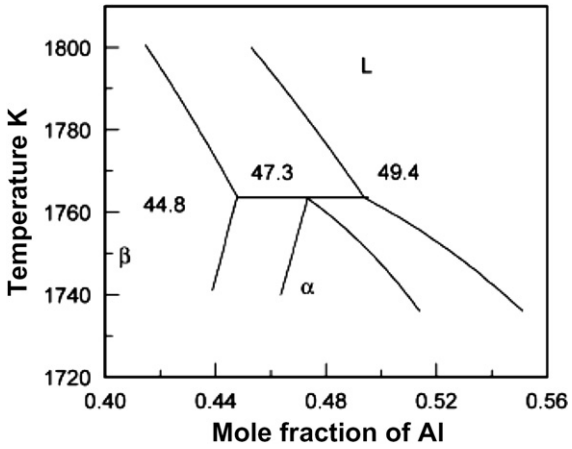

Fig. 2. Phase diagram of Ti–Al system near L + β → α area [11].

Despite the fact that droplets endure the temperature below T_L during undercooling, solidification will not start until nucleation temperature T_N is reached. In this cooling model, heterogeneous nucleation is considered for the droplets due to the fact that major portion of powder particles generated by gas atomisation is over 20 μm [8], in which range heterogeneous nucleation occurs mostly.

The nucleation temperature is obtained as [12]

$$T_N = T_L - \Delta T_{het}. \tag{2}$$

The heterogeneous undercooling ΔT_{het} can be found based on the experimental data in [12] as

$$\Delta T_{het} = \Delta T_{hom} \exp(-2.2 \times 10^{12} V). \tag{3}$$

According to the nucleation theory [13], the maximum homogeneous undercooling ΔT_{hom} for a droplet can be evaluated from

$$\Delta T_{hom}^2 = \frac{16\pi\sigma_m^3 \Omega_V^2 T_L^2}{3k\left(T_L - \Delta T_{hom}\right) H_f^2 \ln\left(10^{44} V \frac{\Delta T_{hom}}{\dot{T}}\right)}. \tag{4}$$

2.1.3. Recalescence

Once the droplet temperature reaches the nucleation temperature, solidification start to progress and the droplets are no longer in complete liquid state, in which case, Eq. (1) is no longer valid. After the nucleation, there is a sudden surge of droplet temperature due to the release of latent heat of fusion, this phenomenon is called recalescence. This period ends when the added internal heat source from the latent heat of fusion is balanced by the rate of heat exchange with the surrounding gas. Now the heat exchange including convection and radiation is expressed as

$$H_f \frac{df}{dt} = \frac{6h}{\rho_p d_p}(T_p - T_g) + \frac{6\varepsilon\sigma_{SB}}{\rho_p d_p}(T_p^4 - T_w^4). \tag{5}$$

The growth rate of solid phase can be modelled with the expression [10]

$$\frac{df}{dt} = \frac{R(T_L - T_p)}{d_p}. \tag{6}$$

The temperature at the end of recalescence T_r (T_p at end of reclascence) can be found by introducing Eq. (6) in Eq. (5):

$$H_f \frac{R(T_L - T_r)}{d_p} = \frac{6h}{\rho_p d_p}(T_r - T_g) + \frac{6\varepsilon\sigma_{SB}}{\rho_p d_p}(T_r^4 - T_w^4). \tag{7}$$

2.1.4. Segregated solidification

Solidification could continue to process within droplets after the recalescence. Two segregated solidifications have been identified for alloy droplets [6], namely initial and further segregated solidifications. The initial segregated solidification takes place after recalescence while the further segregated solidification occurs after peritectic transformation. Both segregated solidifications work in the same principle and the droplet temperature decreases as the solidification processes. The heat exchange can be expressed as

$$\frac{dT_p}{dt}\left[c_{pl}(1-f) + c_{ps}f - H_f\frac{df}{dT_p}\right] = \frac{6h}{\rho_p d_p}(T_p - T_g) + \frac{6\varepsilon\sigma_{SB}}{\rho_p d_p}(T_p^4 - T_w^4). \tag{8}$$

According to Scheil's theory [9] the solid fraction during segregation can be modelled as

$$f = 1 - (1 - f_r)\left(\frac{T_M - T_p}{T_M - T_L}\right)^{\frac{1}{k_e - 1}}. \tag{9}$$

T_M is a reference temperature and is given the value of 2016 K [1] for this particular material and f_r is the solid fraction at the end of recalescence. Derivation of Eq. (9) gives the rate of change of f with temperature as

$$\frac{df}{dT_p} = \frac{1 - f_r}{(k_e - 1)(T_M - T_L)}\left(\frac{T_M - T_p}{T_M - T_L}\right)^{\frac{2 - k_e}{k_e - 1}}. \tag{10}$$

2.1.5. Peritectic transformation

Droplet temperature declines during the initial segregated solidification, but solidification within the droplet continues to progress at a constant temperature once the peritectic temperature is reached. The energy equation is the same as Eq. (5).

Peritectic solidification ends when the composition of the remaining liquid reaches the appropriate concentration. The solid fraction at the end of the Peritectic transformation can be found by lever rule according to the phase diagram in Fig. 2.

$$f_{per} = \frac{0.494 - c_0}{0.494 - 0.473} = 0.67 \quad (\text{for } c_0 = 0.48). \tag{11}$$

2.1.6. Cooling in solid state

The droplet is not fully solidified after peritectic transformation and further segregated solidification finally turns the droplet to a complete solid particle. As the droplet is still much hotter than the surrounding gas, the heat exchange for the solid particle can be expressed as

$$c_{ps}\frac{dT_p}{dt} = \frac{6h}{\rho_p d_p}(T_p - T_g) - \frac{6\varepsilon\sigma_{SB}}{\rho_p d_p}(T_p^4 - T_w^4). \tag{12}$$

The convective heat transfer coefficient h is calculated by the widely used correlation of Ranz and Marshall [14]:

$$h = \frac{k_g}{d_p}(2 + 0.6\sqrt{Re}\sqrt[3]{Pr}), \tag{13}$$

where k_g is the gas thermal conductivity, Re is the Reynolds number $\frac{\rho_g d_p (v_g - v_p)}{\mu_g}$, Pr is the Prandtl number $\frac{c_{pg}\mu_g}{k_g}$ and μ_g is the molecular viscosity of the gas.

2.2. Droplet break-up model

The most significantly improvement from this research work is the integration of droplet cooling with break-up

models while existing droplet models have been used the same droplet size throughout. The droplet break-up model has been described thoroughly in [8] and only some basic equations are given in this section. The break-up model is based on two robust break-up theories, namely TAB [15] and Kelvin–Helmotz (KH) [16] instability. A transition point (Weber number = 80) is set for switching between those two break-up models due to the fact that TAB model is more accurate for low *We* condition and KH model is more suitable for high *We* condition.

2.2.1. TAB model

This model treats the oscillation of distorting droplets with the analogy of a spring-mass system. The restoring force of the spring is represented by the surface tension, while the external force is replaced by aerodynamic force. The liquid viscosity represents the damping forces. Given $y = x/C_b r$ the governing equation becomes

$$\ddot{y} = \frac{C_F}{C_b}\frac{\rho_g}{\rho_l}\frac{u^2}{r^2} - \frac{C_k\sigma}{\rho_l r^3}y - \frac{C_d u}{\rho_l r^2}\dot{y}. \tag{14}$$

The break-up occurs when $y > 1$. The values of constant C_b, C_F, C_k and C_d are determined based on experimental and theoretical results. First the relative velocities of each parcel are calculated with respect to the surrounding gas velocity. The second step is to calculate *We* and the frequency ω is defined as

$$\omega^2 = C_K\frac{\sigma}{\rho_l r^3} - \left(\frac{C_d\mu_l}{2\rho_l r^2}\right)^2. \tag{15}$$

At this point, the oscillation amplitude can be calculated as

$$\Psi^2 = \left(y^n - \frac{We}{12}\right)^2 + \left(\frac{\dot{y}^n}{\omega}\right)^2. \tag{16}$$

The break-up condition is

$$\Psi + \frac{We}{12} \geqslant 1. \tag{17}$$

The break-up time t_b is estimated assuming that the drop oscillation is undamped for its first period (that is true for very small droplets) and is the smallest root greater than t^n of the equation

$$\frac{We}{12} + \Psi\cos\left[\omega(t - t^n) + \phi\right] = 1, \tag{18}$$

where

$$\cos\phi = \frac{y^n - \frac{We}{12}}{\Psi} \quad \text{and} \quad \sin\phi = -\frac{\dot{y}^n}{\Psi\omega} \tag{19}$$

the size of the product droplet is related to the break-up time via an exponential expression

$$r = \frac{d_p}{2} \times \text{decayfactor}, \tag{20}$$

where decay factor is a function of the parent droplet life time until break-up condition is reached.

2.2.2. KH model

This model takes into account the fastest growing disturbance on the surface of the droplet, which is most probable to result in break-up. The wavelength of this disturbance is

$$\Lambda = \frac{9.02(1 + 0.45Z^{0.5})(1 + 0.4\Gamma^{0.7})}{(1 + 0.87We^{1.67})^{0.6}}d_p. \tag{21}$$

The growth rate of the wavelength is

$$\Omega = \frac{(0.34 + 0.38We^{1.5})}{(1 + Z)(1 + 1.4\Gamma^{0.6})}\left(\frac{\sigma}{\rho_l d_p^3}\right)^{0.5}. \tag{22}$$

The droplets radius r resulting from atomization is proportional to the wavelength of the fastest-growing unstable surface wave

$$r = B_0\Lambda. \tag{23}$$

B_0 is a model constant equal to 0.61 based on the Reitz analysis. The break-up time t_b is given by

$$t_b = \frac{3.726B_1}{\Omega\Lambda}. \tag{24}$$

B_1 must be regarded as an adjustable model constant, with a different value in each break-up regime: in the Reitz analysis is assumed $B_1 = 10$. To model the stretching and thinning mechanism of "child" droplets pinching from the "parent" droplet, the diameter evolution law is

$$\frac{dr_p}{dt} = \frac{r_p - r}{t_b}. \tag{25}$$

Further, the parent droplet diameter reduction will take place only after the mass removed (according to Eq. (25)) reaches three percent of its mass.

3. Results and discussion

3.1. Computational domain and gas flow

This close-coupled atomisation process is schematically shown in Fig. 3. During the operation, molten metal is poured into the atomization chamber from the tundish through a ceramic feed tube where a high pressure gas jet comes in contact with the melt. The use of computational scheme and development of computational domain are detailed in [8], therefore only a brief description about the domain is given here. The atomization chamber and the enclosed flow can be treated with a rotational symmetry and only half of an axial section of the atomizer chamber needs to be included in a 2D simulation. The computational domain encompassing the melt and gas flow field is shown in Fig. 4. Structured grid (80,000 cells) is deployed and local refinement is achieved in the zones of high pressure gradients and near the wall. The gas flow velocity field for the tracking of the droplets is shown in Fig. 5. The turbulent flow has a Reynolds number of 800,000. At the exit, the gas flow expands through a series of Prandtl–Meyer

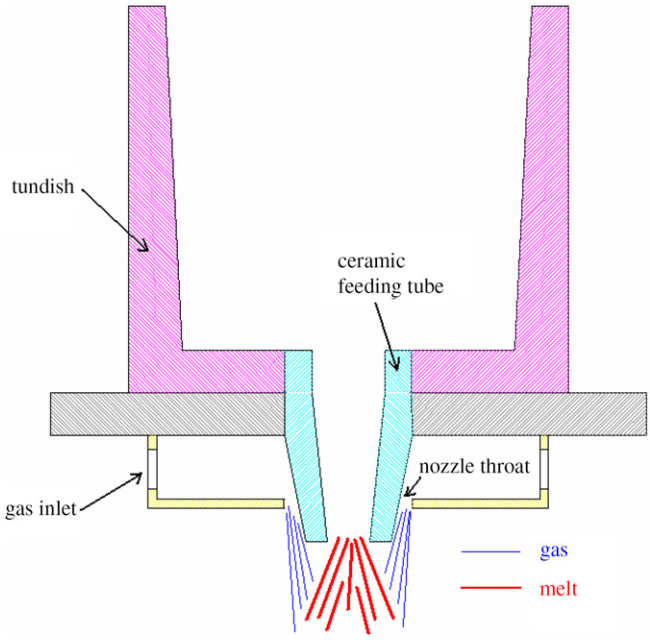

Fig. 3. A schematic of gas atomisation process.

expansion waves [17]. The gas flow separation at the corner of the melt tube generates a recirculation vortex under the melt exit hole. The gas flow in the centre of the recirculation zone moves toward the feeding tube and turns outward radially as it moves close to the tip. At the end of this recirculation zone there is a stagnation front, where the gas velocity falls to around zero. In all simulations γ-TiAl (thermal properties are given in Table 1) droplets are used and the melt superheat at the pouring stage is 100 K above the liquidius temperature 1785 K. The atomising gas is nitrogen and the gas to melt mass flow rate ratio is approximately 1.1. Four simulation results are provided in this paper as shown in Table 2. In Droplet A case, 3 mm droplets are injected at the corner of feeding tube as shown in Fig. 5. The following discussion is based on the results of Droplet A without further notification.

3.2. Heat transfer coefficient

The convective heat transfer coefficient (CHTC) is a function of both droplet diameter and the relative velocity between gas and droplet phases as described in Eq. (13). CHTC increases as droplet diameter decreases and responses positively to the increase of the relative velocity. When the droplets are injected into the domain they are accelerated by expanded nitrogen gas. Fig. 6 shows the behaviour of the relative velocity between gas and droplet. At the beginning, the droplets are accelerated as they come into contact with the external surface of nitrogen jet, subsequently the relative velocity decreases as shown in region 1. When the droplets pass through the external mixing layer (between expanded nitrogen and still air) and enter the jet core, the relative velocity suddenly increases as shown in region 2. After this, the relative velocity decreases as the carrying gas accelerates the droplets further as shown in region 3. The change of the droplet diameters as a result of break-up is depicted in Fig. 7. The droplet size declines rapidly in regions 1 and 2 and reaches a stable size of ~80 μm at Region 3. A detailed description of droplet break-up history can be found in [8].

The combined effects on CHTC are shown in Fig. 8. CHTC starts at a low value due to large droplet size, increases in regions 1 and 2, follows by a surge in region 3 as both relative velocity and droplet size decrease rapidly. CHTC peaks when the droplets stop to break further. From that point on, CHTC develops accordingly to the relative velocity as the droplet size keeps constant. CHTC

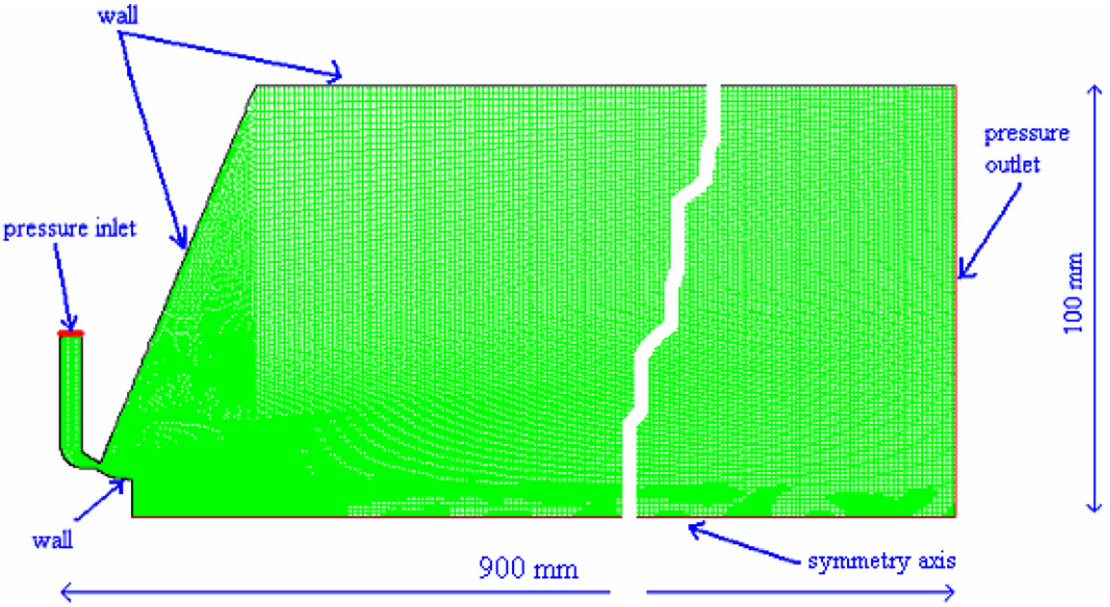

Fig. 4. Compuational grid and boundary conditions.

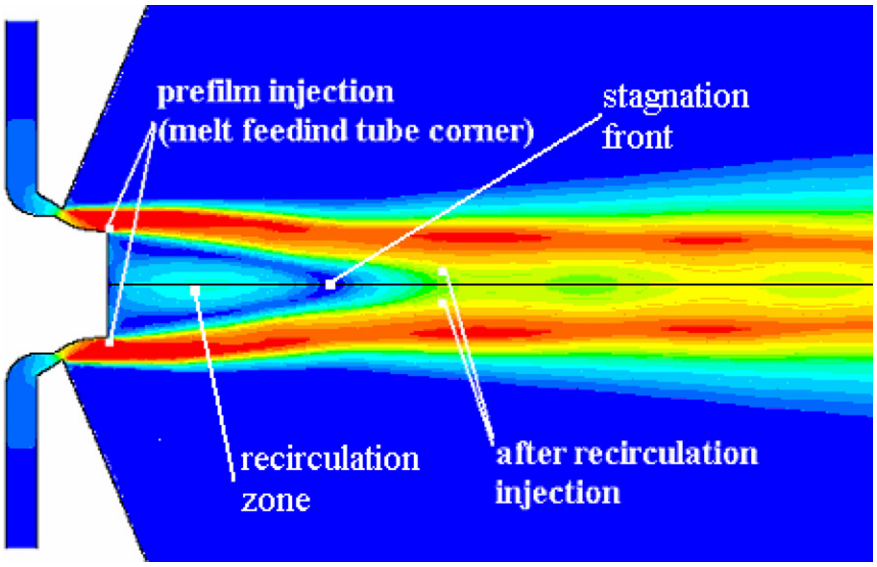

Fig. 5. Gas velocity contours showing flow pattern within atomisation areas.

Table 1
Melt material properties [1]

Parameter	Value	Unit
c_g	519	J kg^{-1} K^{-1}
c_{pl}	829	J kg^{-1} K^{-1}
c_{ps}	727	J kg^{-1} K^{-1}
H_f	28,270	J mol^{-1}
k_e	0.74	–
k_g	0.01636	W m^{-1} K^{-1}
R	0.01	m s^{-1} K^{-1}
T_i	1885	K
T_L	1785	K
T_M	2016	K
T_{per}	1764	K
μ_g	1.7×10^{-5}	kg m^{-1} s^{-1}
ρ_p	3636	kg m^{-3}
σ_m	203.4×10^{-3}	J m^{-2}
Ω	2.08×10^{-5}	M^3 mol^{-1}

Table 2
Droplets performed in simulation

Simulation cases	Droplet size at injection (diameter – mm)	Injection location	Droplet size at exit of domain (diameter – μm)
Droplet A	3	Feeding tube corner	82
Droplet B	5	Feeding tube corner	152
Droplet C	1	Feeding tube corner	22
Droplet D	5	Stagnation point	213

declines to the minima as the relative velocity drops toward zero (transition from acceleration to deceleration). In the final part, CHTC gradually increases according to the relative velocity. Throughout the entire simulation domain, the CHTC is very high ($>10^3$ W/m^2 K). The predicted value and development are consistent with the modelling results in a similar system reported in [3].

3.3. Thermal history and solidification

As shown in Fig. 9, the temperature of droplets declines slowly at the beginning in almost linear fashion. At the point P1, droplets start to break down to smaller size which improves both acceleration and heat transfer rate. As a result, particle temperature declines rapidly till the nucleation temperature (1550 K) is reached at the point P2, where the solidification takes place. From the point P2, the recalescence produces a fast rise in particle temperature. This is due to the fact that the external cooling of the drop (convection) is not able to remove the heat released from the particle interior due to latent heat of fusion. The correlation between solidification and particle temperature is evident as shown in Fig. 9. From the start to the point P2, the particle is in full liquid state. Solidification mainly takes place during recalescene and at the end of recalescence (the point P3) almost 70% of the particle is solid. After recalescence, particles solidify gradually following segregated solidification, Peritectic transformation and segregated solidification. For Droplet A with initial diameter of 3 mm, particles leave the computational domain before fully solidified (~90%).

3.4. Effect of droplet size

In order to quantify the effects of initial droplet size on cooling behaviour, two additional sizes of droplets are injected at the corner of feeding tube, namely 5 mm (Droplet B) and 1 mm (Droplet C) diameters. The relative velocities (Fig. 10) and the change of particle size (Fig. 11) among these three droplets have very similar profiles. The history of CHTCs in Fig. 12 among those droplets shows a certain degree of resemblance, however, the smaller initial droplet size is, the higher CHTC is achieved, which is particular for Droplet C (1 mm). The effects of initial droplet

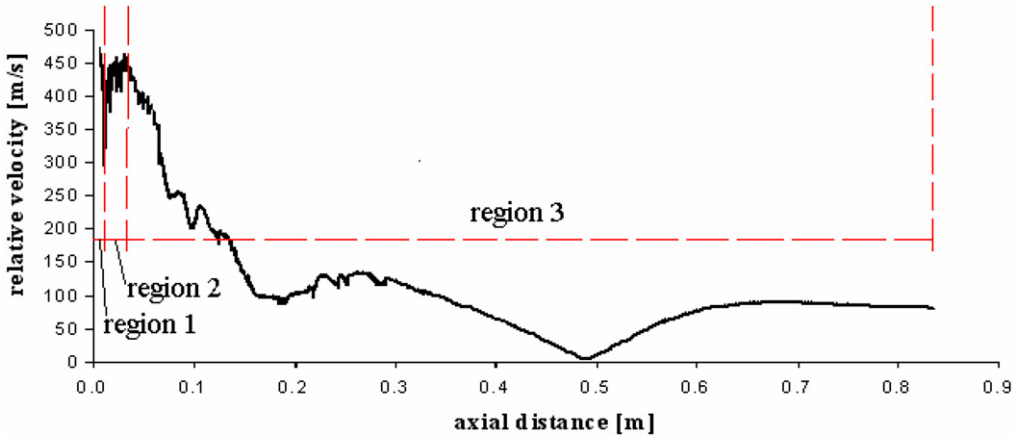

Fig. 6. Relative velocity profile from Droplet A.

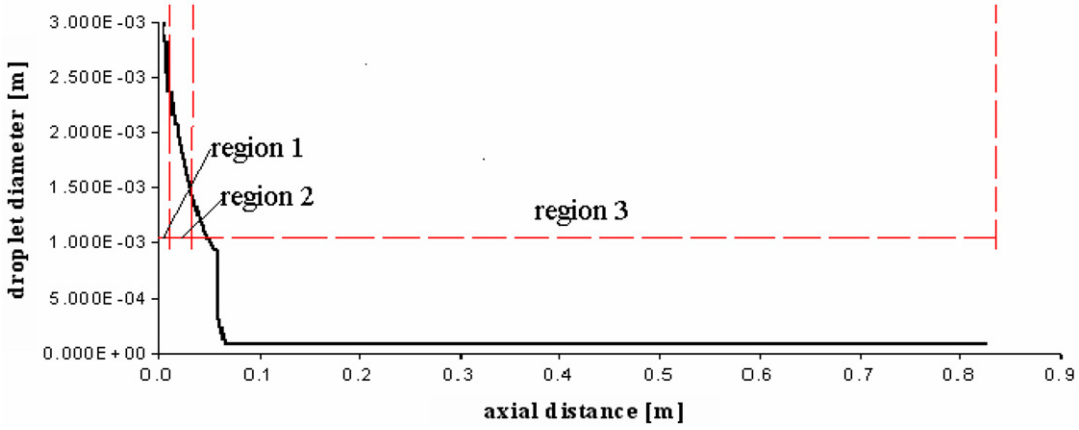

Fig. 7. Change of particle size from Droplet A.

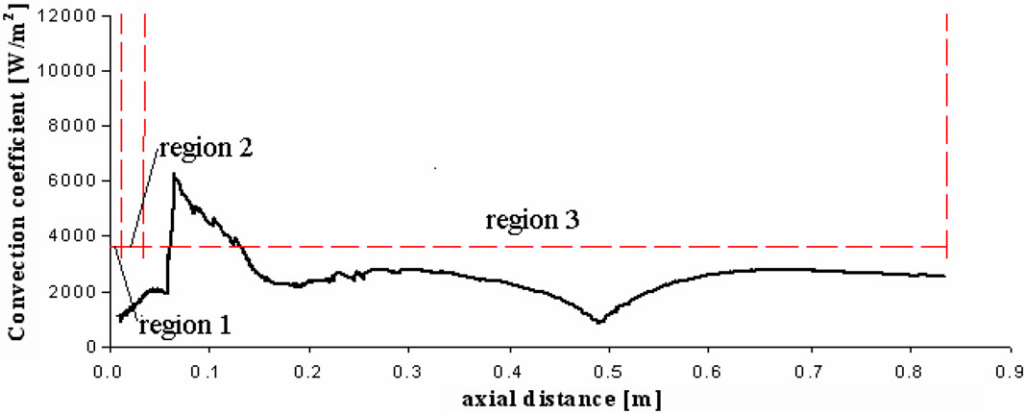

Fig. 8. Heat transfer coefficient profile from Droplet A.

size on the particle thermal and solidification history are clearly demonstrated in Figs. 13 and 14. For small Droplet C (1 mm), solidification is complete during recalescence and particle temperature declines rapidly after recalescene as fast cooling takes place in solid. The prediction is consistent with the experimental observation in [18], which found that solidification was complete during recalescence when the nucleation undercooling was greater than the hypercooling limit (h_f/c_{pl}). The results from Droplet C show that the particles are reduced to sizes of (~20 μm) after breakup with a hypercooling limit about 328 K and undercooling around 420 K, which values are consistent with the predictions on similar particle sizes reported in [1]. For large Droplet B (5 mm), no undercooling is found from

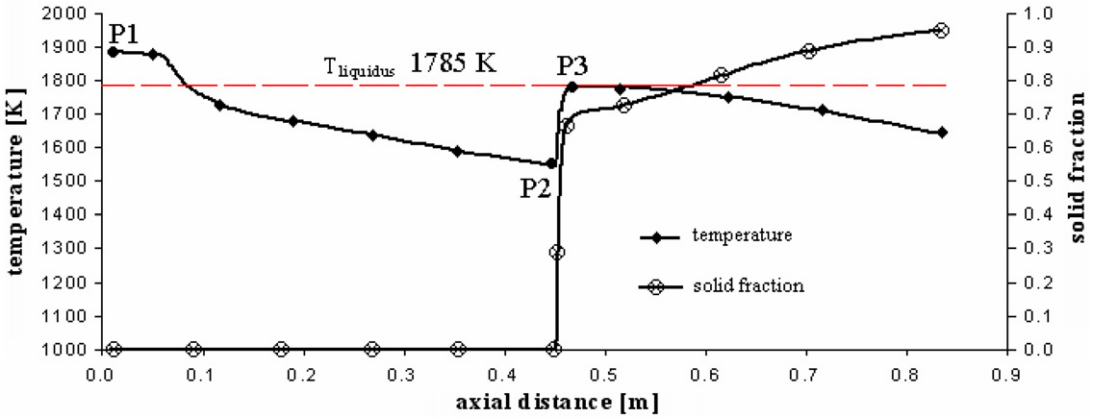

Fig. 9. Particle temperature and solidification profile from Droplet A.

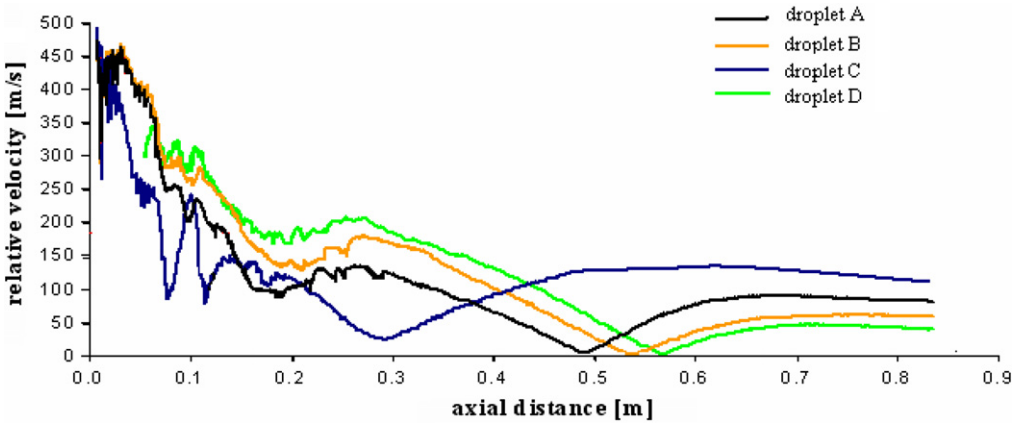

Fig. 10. Relative velocity profile from Droplets A – D.

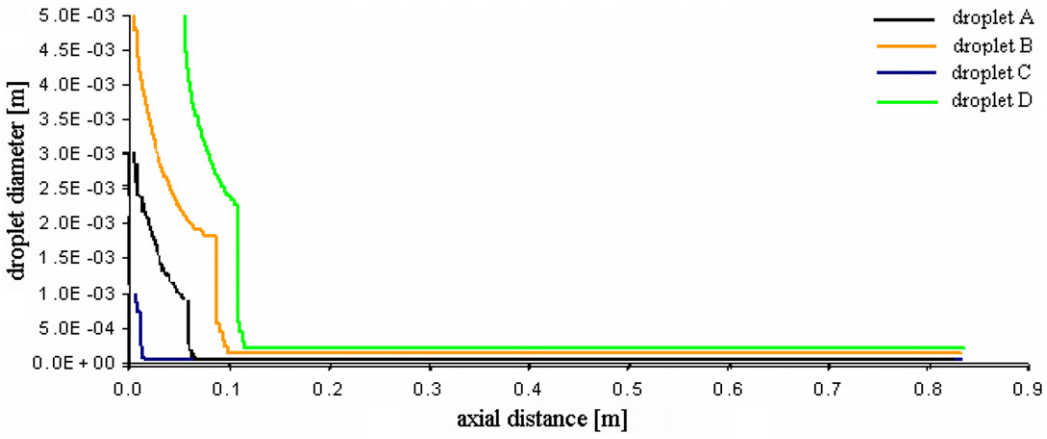

Fig. 11. Change of particle diameter from Droplets A – D.

the simulation results and the particles only solidify ~50% at the end of computational domain.

3.5. Effect of injection locations

According to experimental observation on similar systems [19], small droplets are seen at the corner of the melt feeding tube and large droplets appear flowing down from the recirculation zone. It is believed that prefilming will push the melt along the radius of feeding tube and generate small droplets at the corner. The droplets flowing down directly from the feeding tube have not gone through the pre-filming and large droplets are formed as a result after the recirculation zone. In this paper, large droplets with

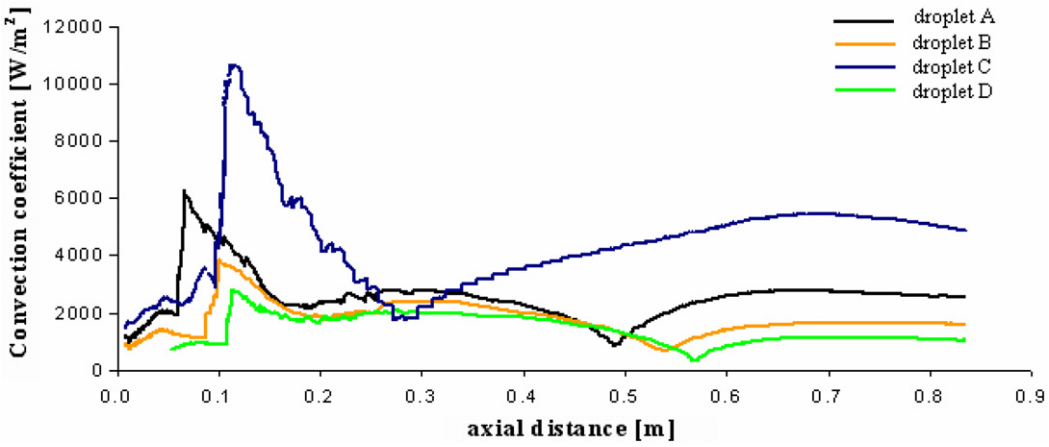

Fig. 12. Heat transfer coefficient profiles from Droplets A – D.

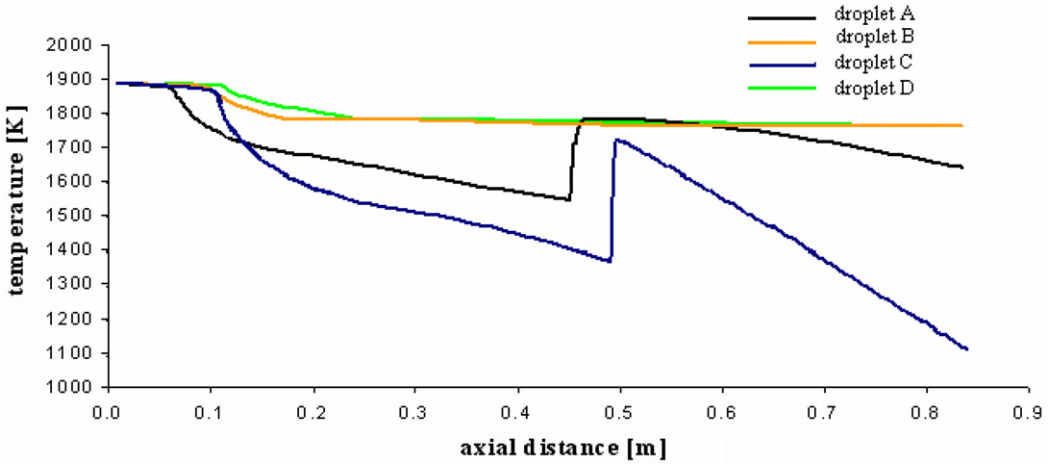

Fig. 13. Temperature profiles from Droplets A – D.

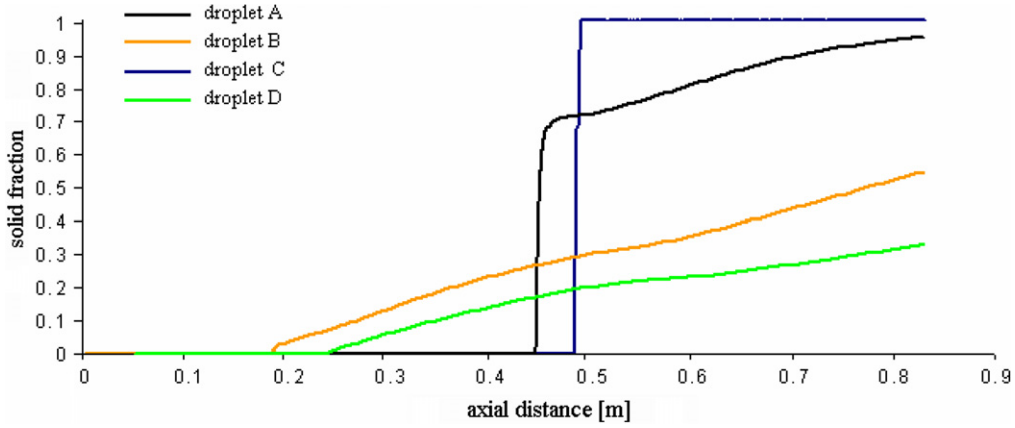

Fig. 14. Solid fraction profiles from Droplets A – D.

initial diameter of 5 mm are released after the recirculation (Droplet D) as shown in Fig. 5. The comparisons between the after recirculation and corner injections are shown in Figs. 10–14. In the case of same droplet size (Droplets B and D), the profiles of their variables throughout the domain are very similar apart from a shift of displacement (~10 cm). These results indicate the atomisation and solidification process of droplets are closely related to in-flight distance rather than their initial locations in the gas flow generated during gas atomisation. It needs to point that, the use of 5 mm droplets at both locations are only for quantitative comparison. In reality, smaller droplets

emerge from the corner of feeding tube as a result of prefilming and large droplets flow down from the recirculation zone, therefore, droplets from the corner are expected to atomised and solidified in greater extent than droplets from the recirculation zone. The simulation results confirm a widely employed approach to improve the atomisation process, i.e., to increase the length of atomisation tower, which will allow the droplets break further and solidify more before pile-up at the bottom of atomisation tower. When hot metal powders accumulate at the bottom of atomisation tower, they may solidify further into bulk metal, which phenomena need to be avoided during atomisation practice. The extension of atomisation tower's length could effectively reduce that incidents and improve product yield.

4. Conclusions

A modified model has been developed for the cooling and solidification of metal droplets. The droplet model incorporates the detailed heat transfer mechanism of undercooling, recalescence, peritectic and segregated solidification, which can be used to accurately predict thermal-physics of metal powders in process engineering. The major advantage of this model is its ability to combine both cooling and break-up in the same computation. The models were employed to analyze the gas atomisation process for powder production. A summary of the results is as follows.

1. The thermal history of droplets is strongly dependent on initial droplet size which is closely related to droplet acceleration, cooling and break-up process,
2. Solidification mainly takes place during recalescence. For small droplets which have the nucleation undercooling greater than the hypercooling limit, solidification completes during recalescence and follows by rapid decline of particle temperature. Otherwise, particles continue to solidify slowly after recalescence.
3. Droplets have very similar profiles during gas atomization and the major factor influencing the atomization and solidification process of droplets is in-flight distance.

References

[1] B. Li, X. Liang, J.C. Earthman, E.J. Lavernia, Two dimensional modelling of momentum and thermal behaviour during spray atomization of –TiAl, Acta Mater. 44 (6) (1996) 2409–2420.
[2] H. Liu, R.H. Rangel, E.J. Lavernia, Modelling of droplet–gas interaction in spray atomization of Ta–2.5W alloy, Mater. Sci. Eng. A 191 (1995) 171–184.
[3] J.P. Delplanque, E.J. Lavernia, R.H. Rangel, Analysis of in-flight oxidation during reactive spray atomization and deposition processing of aluminium, J. Heat Transfer 122 (2000) 126–133.
[4] P. Shukla, R.K. Mandal, S.N. Ojha, Non-equilibrium solidification of undercooled droplets during atomization process, Bull. Mater. Sci. 24 (2001) 547–554.
[5] J.H. Hattel, N.H. Pryds, J. Thorborg, P. Ottosen, A quasi-stationary numerical model of atomized metal droplets. I: Model formulation, Modell. Simulat. Mater. Sci. Eng. 7 (1999) 413–430.
[6] D. Bergmann, U. Fritsching, K. Bauckhage, A mathematical model for cooling and rapid solidification of molten metal droplets, Int. J. Therm. Sci. 39 (2000) 53–62.
[7] R.P. Underhill, P.S. Grant, B. Cantor, D.J. Bryant, Modelling of droplet behaviour during spray forming using Fluent, Int. J. Non-equilib. Process. 10 (1997) 201–216.
[8] N. Zeoli, S. Gu, Numerical modelling of droplet break-up for gas atomisation, Computat. Mater. Sci. 38 (2) (2006) 282–292.
[9] E. Scheil, Uber die eutektische kristallisation, Zeitschrift für Metallkunde 34 (1942) 70–80.
[10] FLUENT 6.2, Fluent Europe, Sheffield Business Park, Europa Link, Sheffield S9 1XU, UK.
[11] Y. Su, C. Liu, X. Li, J. Guo, B. Li, J. Jia, H. Fu, Microstructure selection during the directionally peritectic solidification of Ti–Al binary system, Intermetallics 13 (2005) 267–274.
[12] P. Mathur, D. Apelian, A. Lawley, Analysis of the spray deposition process, Acta Metall. Mater. 37 (1989) 429–443.
[13] J.P. Hirth, Nucleation, undercooling and homogeneous structures in rapidly solidified powders, Metall. Trans. A 9 (3) (1978) 401–404.
[14] W.E. Ranz, W.R. Marshall, Evaporation from drops (part 1 and 2), Chem. Eng. Progr. 48 (1952) 141–146.
[15] P.J. O'Riyrje, A.A. Amsden, The TAB method for numerical calculation of spray droplet breakup, SAE Technical Paper 872089, 1987.
[16] R.D. Reitz, Modelling atomisation processes in high-pressure vaporizing sprays, Atomisation Spray Technol. 3 (1987) 309–337.
[17] J.D. Anderson, Modern Compressible Flow with Historical Perspective, third ed., McGraw-Hill, Boston, 2003.
[18] B.Cantor, Microstructure development during rapid solidification, in: Proceedings of the 22nd Risø International Symposium on Materials Science, Roskilde, Denmark, 2001, pp. 483–493.
[19] S.P. Mates, G.S. Settles, A study of liquid metal atomization using close-coupled nozzles, part 1 and 2, Atomization Sprays 15 (2005) 19–40.